Collagen and Leather

RESEARCH

Open Access

Injectable hyaluronate/collagen hydrogel with enhanced safety and efficacy for facial rejuvenation

Lu Song[1], He Qiu[2], Zhiru Chen[1], Jing Wang[1], Yang Xu[1], Zhanhong Liu[1], Shuo Liu[1], Zhiyuan Wang[1], Xiangdong Zhu[1], Kai Zhang[1], Hai Lin[1*] and Xingdong Zhang[1]

Abstract

Collagen, known for its excellent biocompatibility and biological properties, has limited in vivo maintenance duration after implantation, while hyaluronic acid faces challenges such as various complications and insufficient support for cell proliferation. In this study, an injectable hyaluronic acid/collagen (HCol) hydrogel was developed to achieve enhanced cell-material interactions and accelerated skin regeneration. Physical and chemical characterizations demonstrated that the HCol hydrogel was injectable and stable after the implantation. In vitro cell culture results illustrated that the hydrogel promoted the proliferation of human dermal fibroblasts, extracellular matrix expression and angiogenesis. The subcutaneous implantation in rats showed the superior biocompatibility of HCol hydrogel and enhanced secretion and deposition of extracellular matrix, compared with commercial hyaluronic acid dermal filler. MRI analysis showed that the hydrogel stably remained in vivo for at least three months. The histological examination and SHG signals further demonstrated that the hydrogel modulated fibroblast phenotype and stimulated vascular ingrowth and collagen synthesis, without inducing significant inflammation, swelling or erythema in vivo.

Keywords Collagen hydrogel, Hyaluronic acid, Cell phenotype, Subcutaneous implantation, Collagen regeneration

*Correspondence:
Hai Lin
linhai028@scu.edu.cn; ohai3@163.com
Full list of author information is available at the end of the article

Graphical Abstract

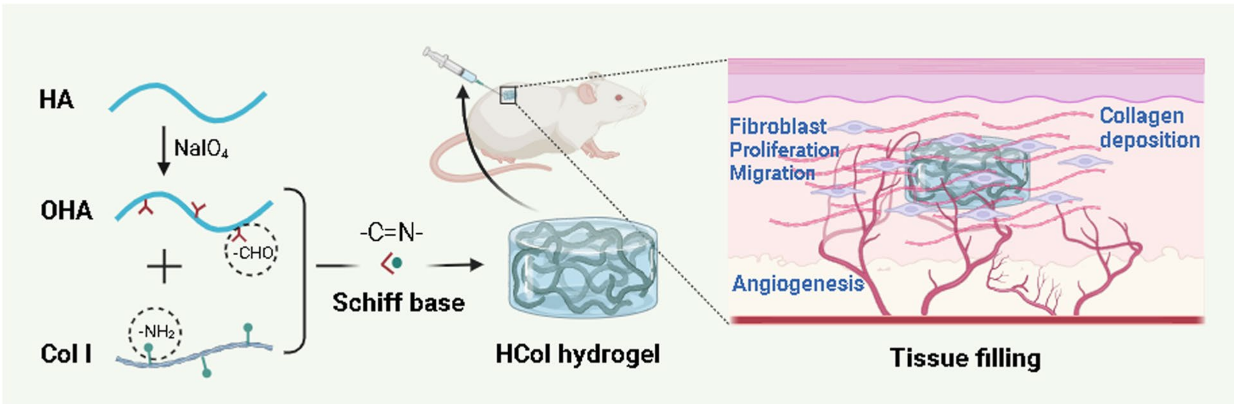

1 Introduction

In recent years, progress in understanding the mechanisms of facial aging has driven the development of minimally invasive surgery in the field of facial rejuvenation [1]. Dermal fillers can be used in simple and short procedures for surgery and rapid facial rejuvenation, leading to an increasing focus on using fillers to expand tissues and improve skin aesthetics [2]. An ideal dermal filler should be safe, affordable, hypoallergenic, easy to store and distribute, provide quick and painless injections, require no allergy testing, have minimal risk of complications, and offer natural, long-lasting, consistent, predictable results that can be easily removed if needed [3]. Though no filler currently meets all these criteria, the market is expanding with new technologies and products. Current dermal filler products can be classified into two catalogs according to their biodegradability in vivo, that is non-biodegradable and biodegradable. Non-biodegradable fillers have long-lasting effects (5 years to more permanent), such as liquid silicone and PMMA (poly-methyl methacrylate) [4, 5]. On the contrary, biodegradable fillers have temporary effects (3 to 24 months) and require regular injections, such as PLLA (poly-L-lactic acid) and CaHA (calcium hydroxyapatite) (long-lasting, 15–24 months), as well as collagen and HA (medium-lasting, 3–12 months) [4–6].

Collagen plays a critical role in maintaining the structure and integrity of skin, as well as combating the effects of aging. Comprising 85–90% of the skin's dry weight, collagen is essential for maintaining skin elasticity [7, 8]. However, the aging process leads to various changes in the skin, including rough texture, wrinkles, spots, and atrophy, resulting in the loss of tissue integrity [9–11]. The biosynthesis ability of collagen in fibroblasts diminishes over time, causing the destruction and collapse of the extracellular matrix, and contributing to skin aging [12, 13]. The implantation of collagen was considered one of the effective strategies to improve extracellular matrix conditions and postpone skin aging.

Hyaluronic acid (HA) is the most abundant glycosaminoglycan found in the dermis. It is present in the extracellular matrix of the skin, ocular vitreous body, and articular cartilage [14]. HA is highly hygroscopic, capable of binding water up to 1000 times its weight. This property enables HA to contribute to tissue hydration, volume, and structural support [15]. As an important component of the extracellular matrix, HA's exceptional water retention capacity and biodegradability allow for its use in cosmetics, drug delivery systems and skin defect repair [16–18]. HA-based hydrogels have become the most commonly used soft-tissue fillers for facial rejuvenation [16]. However, HA fillers may trigger allergic reactions due to the presence of hyaluronan-related proteins and BDDE (1, 4-butanediol diglycidyl ether) [2, 19], including vascular occlusion, inflammation, erythema, oedema, itching, and pain [1, 2]. New research indicated that increased polysaccharide modifications reduce the biocompatibility of HA-based materials [19, 20]. Overall, the development of dermal fillers continues to progress, with collagen and hyaluronic acid playing pivotal roles in maintaining facial rejuvenation.

This study focused on an injectable hydrogel composed of hyaluronic acid and type I collagen (HCol), specifically engineered to provide physical support and enhance tissue regeneration. The hydrogel was synthesized using moderate chemical crosslinking and analyzed their safety and efficacy both in vitro and in vivo. The HCol hydrogel was prepared with optimized parameters, and the physicochemical properties were characterized. In addition, the cell behaviors in HCol hydrogel were studied and the in vivo stability and promotion of skin regeneration were investigated using a rat subcutaneous implant model.

2 Materials and methods

2.1 Materials

Type I collagen was extracted and purified from newborn calfskin in our laboratory. Sodium hyaluronate (HA, 200–400 kDa) was purchased from Bloomage Biotech (Jinan, China). Acetic acid (HAC), sodium hydroxide (NaOH) and sodium periodate ($NaIO_4$) were purchased from Kelong Reagent Company (Chengdu, China). Human skin fibroblast cell (HSF) was purchased from Saibaikang Biotechnology Co., Ltd (Shanghai, China). Dulbecco's Modified Eagle Medium (DMEM, high glucose) was purchased from Servicebio (Wuhan, China). Fetal bovine serum (FBS, Gibco, Australia origin) was bought from Thermo Fisher Scientific Corporation (USA). Sigma-Aldrich (USA) provided the following chemicals: rhodamine-phalloidin, propidium iodide (PI), fluorescein diacetate (FDA), and 4′6-diamidino-2-phenylindole (DAPI). Cross-linked Sodium Hyaluronate Gel for injection (CHA) (Matrifill®, Approval No. 20,173,130,810) was purchased from Qisheng Biological Preparation Co., Ltd, Shanghai. All compounds were utilized as received without any additional processing unless otherwise indicated.

2.2 Preparation and characterization of HCol hydrogels

2.2.1 Modification of hyaluronic acid

Modification of sodium hyaluronate with sodium meta periodate as previously reported [21]. Briefly, a 1% (wt) sodium hyaluronate solution was prepared by dissolving 1.5 g sodium hyaluronate in 150 mL deionized water. Then, 1.86 mL of 0.5 M sodium metaperiodate was added dropwise to the solution. After reacting in the dark for 24 h, the reaction was terminated by adding 5 times the volume of ethylene glycol. The reaction mixture was then placed in a dialysis bag with a molecular weight cutoff of 8000–14,000 Da and dialyzed against deionized water for 3 days, and the water was changed three times a day. After the dialysis, the product was freeze-dried to obtain the oxidated hyaluronic acid derivative (OHA), which was stored at 4 ℃ before further study. The oxidation degree of OHA was characterized by the hydroxylamine hydrochloride method [22].

2.2.2 Fabrication of HCol hydrogels

Pepsin was used to extract type I collagen (Col I) from calfskin, and it was then stored at a concentration of 25 mg/mL in 0.5 M acetic acid (HAC). During the preparation, the collagen was chemically sterilized under the sterility process control protocol. A 5 M sodium hydroxide (NaOH) solution was added to the collagen solution while it was submerged in an ice bath to bring its pH up to 7.2–7.4. The following procedures were manipulated under aseptic conditions to get sterile gels.

To obtain sterile OHA, the OHA was soaked in 75% ethanol for 24 h, rinsed three times with deionized water, and then dissolved and freeze-dried. According to the ratio in Table 1, a certain amount of OHA was dissolved in PBS solution. The OHA solution was then injected into a neutral 25 mg/ml Col I solution under ice bath conditions and the pH was further adjusted to neutral following thorough mixing. Finally, the mixture was injected into a mold (d: 8 mm, h: 2 mm) and self-assembled at 37 ℃ for 30 min, resulting in HCol hydrogels with different collagen concentrations. The fluorescence spectrophotometry method based on o-phthalaldehyde (OPA) was used to test the reduction of -NH_2 which reflected the degree of cross-linking [23, 24].

2.2.3 Fourier transform infrared spectroscopy identification

Attenuated total reflectance-Fourier transform infrared (ATR-FTIR) spectra of the lyophilized HA, OHA, Col20, and HCol20 hydrogel were recorded using Nicolet iS50 (Thermo Fisher, USA) in the range of 4000–400 cm^{-1}. Each spectrum was taken as the average of 16 scans at a resolution of 4 cm^{-1}.

2.2.4 Morphology observation

To study its microstructure, HCol hydrogels were prepared as samples for scanning electron microscopy (SEM, HITACHI S-800, Japan) examination by being frozen in fluid nitrogen. The cross-segments of the samples were produced and then sputter-covered with a gold layer.

2.2.5 Swelling measurement

Lyophilized hydrogels in three copies were immersed in PBS solution at different periods to attain equilibrium for the swelling investigations, the gels subsequently were weighed attentively following the removal of the solution on the surface. The equilibrium swelling ratio was given by (Ws-Wd)/Wd, where Ws and Wd stand for the weights of the swollen gel and the dried gel, respectively.

Table 1 Compositions of the HCol hydrogels

Hydrogel name	OHA (ml, 2.87%)	PBS (ml, PH = 7.4)	Col I (ml, 2.5%)
Col20	0	0.4	1.6
HCol10	0.4	0.8	0.8
HCol20	0.4	0	1.6

2.2.6 Dynamic rheological measurement

Dynamic rheological measurements were performed on a Rotational Rheometer (MCR302, Anton Paar, Germany) using a parallel plate geometry (25 mm diameter). The gap between the plates was set at 1 mm in all tests. The strain amplitude sweep mode was applied for HCol hydrogels with a fixed frequency of 10 rad/s and the strain range was from 0.1–1000%. The frequency sweeps for the hydrogels were conducted within the linear viscoelastic region using a constant strain of 1% at 25 ℃ and the frequency range was from 1 to 100 rad/s. Elastic modulus (G') and viscous modulus (G") were recorded as a function of frequency.

2.3 In vitro cell culture

2.3.1 Culture of HSF

1% antibiotic/antimycotic (HyClone, USA), 15% fetal bovine serum (FBS), and 1% sodium pyruvate solution (Gibco, Thermo Fisher, USA) were added to DMEM for the cultivation of HSFs. Cells were cultivated at 37 °C in a humidified environment with 5% CO_2. Adherent cells were harvested and passaged after they reached an 80–90% density.

2.3.2 Cell viability, proliferation and morphology

Following the preparation of OHA/Col I and pH neutrality, the mixture was evenly injected into a 48-well plate (Servicebio, Wuhan, China) to cover the bottom of each well (0.15 mL per well, h = 2 mm), and incubated at 37 ℃ for 30 min to form hydrogels. Healthy HSFs were seeded on the surface of the hydrogel in 500 μL culture medium at a density of 2×10^4 cells/mL and cultured under identical conditions with a change of medium every two days. Propidium iodide (PI) and fluorescein diacetate (FDA) were employed to test the vitality of HSFs after culturing for 1, 3 and 7 days. In short, the samples underwent three PBS rinses and were submerged in a PBS solution that contained 5 μg/mL of FDA and 5 μg/mL of PI for 3–5 min. The samples were then observed using a confocal laser scanning microscope (CLSM, ZEISSLSM 880, Germany). Concurrently, following the manufacturer's instructions, cell counting KIT-8 (CCK-8) was used to assess cell proliferation at the same time intervals. After the cells/hydrogel constructs were obtained, they were brooded for 2 h at 37 °C and 5% CO_2 in a 10% (v/v) CCK-8 solution. A fresh 96-well plate was filled with 100 μL of the supernatant, which was then measured at 450 nm using a microplate reader (Varioskan Flash, Thermo Flasher Scientific, USA).

Using F-actin fluorescence labeling and SEM, the morphology of cells in samples was analyzed at the specified time. Samples were cleaned with PBS, set in 4% (w/v) paraformaldehyde for 30 min at 25 °C, penetrated with 0.5% (v/v) TritonX-100 (Sigma-Aldrich, USA) for 5 min, and afterwards cleaned with PBS multiple times to perform F-actin fluorescence staining. Next, these samples were stained at 25 °C for 1 h in rhodamine-phalloidin solution (5 μg/mL, Sigma-Aldrich) and for 5 min using DAPI (10 μg/mL, Sigma-Aldrich). The models were then cleaned with PBS and observed using the CLSM. For SEM observation, the cells/hydrogel constructs were immersed in 4% (w/v) paraformaldehyde for 24 h as described above. After that, samples were gradually dehydrated for 20 min at a time, with the percentage of ethanol improving to 30%, 50%, 70%, 90%, and 100% (v/v). After being dried using a critical point dryer (LeicaEM CPD300, Germany), the samples were covered with gold in an ion sputter and finally observed by SEM.

2.3.3 Gene expression determined by real-time quantitative PCR (RT-qPCR)

Healthy HSFs were seeded on the surface of the hydrogel at a density of 2×10^5 cells/mL. After being cultured in vitro for 7 and 14 days, type I, IV collagen (Col I, Col IV), vascular endothelial growth factor (VEGF), basic fibroblast growth factor (bFGF), and transforming growth factor beta (TGFβ1) expressions were examined using RT-qPCR. Total RNA was extracted using TRIzol (TRI Reagent, Thermo Fisher, USA). Using the Revert Aid RT Reverse Transcription kit (Accurqte Biology, Hunan), total RNA (1 μg) was reverse transcribed to provide cDNA template for PCR amplification. Synthetic primers (Table 2) for RT-qPCR analysis were made by Qingke Biology (Chengdu, China). The instruction manual's suggested course of action was followed when using thermal cycling. RT-qPCR was carried out using 2×EasyTaq® PCR SuperMix (TransGen Biotech, Beijing, China) and the CFX96TM real-time PCR detection equipment (Bio-Rad, USA). The 2-CT approach was used

Table 2 Primer sequences for the RT-qPCR analysis

Gene	Primer sequences
GAPDH	Forward: 5'-GCCAAGGCTGTGGGCAAGGT-3' Reverse: 5'-AGGTGGAGGAGTGGGTGTCG-3'
Col I	Forward: 5'-GAGAGCATGACCGATGGATT-3' Reverse: 5'-CCTTCTTGAGGTTGCCAGTC-3'
Col IV	Forward: 5'-AGGTGTCATTGGGTTTCCTG-3' Reverse: 5'-GGTCCTCTTGTCCCTTTTGTT-3'
VEGF	Forward: 5'-GGCTCTGAAACCATGAACTTTCT-3' Reverse: 5'-GCAGTAGCTGCGCTGGTAGAC-3'
bFGF	Forward: 5'-TTTTCAGTCTTCGCCAGGTCA-3' Reverse: 5'-TTCGGCAACAGCACACAAATC-3'
TGFβ1	Forward: 5'-GAGAAGAACTGCTGCGTGCGG-3' Reverse: 5'-GCGTGTCCAGGCTCCAAATGT-3'

to determine each targeted gene's level of gene expression. To provide an internal control for measurement, the target gene's mRNA expression levels were standardized to the housekeeping gene GAPDH.

2.4 In vivo evaluation of HCol hydrogels

2.4.1 Surgical procedure

The Experimental Animals Ethics Committee at Sichuan University accepted the animal study (No. K2023011). For the in vivo study, 45 male SD rats (Chengdu Dossy Experimental Animals Co., Ltd.) weighing 200–250 g at 8 weeks of age were utilized. Before the surgery, all of the rats were kept in an animal laboratory setting with a 12-hour light/dark cycle, 22–24 ºC, and 50% humidity for 7 days. Cross-linked Sodium Hyaluronate Gel for injection (CHA) was deemed as the control group. The rats were randomly assigned into five groups (i.e., blank, Col20, HCol10, HCol20 and CHA groups).

Animals were anaesthetized with 4% isoflurane (Friends Honesty Scientific Co., Ltd, China), maintained at 2% during the injections. A subcutaneous implantation model was established in all rats, which had a diagram shown in Fig. 3A. Briefly, a 5*5 cm operative area was obtained after shaving and disinfection. For each rat, six separate injections from the same implant were performed in the dorsal subcutaneous tissue on either side of the spine, and no sutures were required, respectively ($n=3$). In the blank group, no additional biomaterial was implanted. After the injection, the animals were kept in individual cages in the same housing condition as before. Standard balanced food and water were available for free intake.

2.4.2 General observation and MRI analysis

At relevant time points after injection (1 day, 1 month, 2 months, and 3 months), the general aspect of the animals was assessed, including the appearance of the injection sites and the motor behavior.

A custom-designed 32-channel Head coil was positioned at the injection site to facilitate the acquisition of magnetic resonance imaging (MRI) data. The Unity console, equipped with a 3.0T magnet and a 42 mT/m gradient coil from United Imaging (Shanghai, China), was utilized. Imaging parameters were generated using a spin-echo sequence with a repetition time of 17.4 ms and an echo time of 3.9 ms. A 352 × 230-pixel acquisition was performed, yielding a volume of 0.78 × 0.63 × 1.1 mm.

Rats were put in the coil supine for scanning after being anaesthetized with 1% pentobarbital (30 mg/kg). Every month, three rats were scanned to acquire three separate images for each group. The BeeViewer program examined the images to recognize the material-affected area and to measure and rebuild the 3D volume for each sample.

2.4.3 Histological observation and quantitative analysis

1, 2 and 3 months after the injections, the rats were sacrificed with a 150 mg/kg dose of sodium pentobarbital. Each rat's six injected samples were collected alongside some of the surrounding subcutaneous tissue. The samples were treated by paraffin embedding according to conventional histology protocols after being fixed for 24 h at 4 °C in 4% paraformaldehyde. Subsequently, the sections underwent a 5 μm cut using the Exakt Micro-Grindin System (Leica, Germany) and were stained with Masson trichrome (Masson) and hematoxylin and eosin (HE) for histological examination.

2.4.4 SHG signal acquisition

The acquired samples were prepared into 5 μm sections using the above-mentioned method in 2.4.3, then stained with DAPI for SHG signal acquisition. The slices were fixed on the objective stage of a two-photon microscope. A 10X objective was used for scanning, with an excitation wavelength of 950 nm and a laser intensity of 14%. The light was collected using a 465–485 nm narrowband filter. The slices were scanned to a depth of 4 μm in the Z-axis, with a collection speed of 2.44 μm/pixel.

2.5 Statistical analysis

The presentation of all data is mean ± standard deviation ($n \geq 3$). Unless otherwise specified, one-way ANOVA was employed for statistical analysis. $^{*}p<0.05$, $^{**}p<0.01$, $^{***}p<0.001$, and $^{****}p<0.0001$ were deemed as the thresholds for significant differences between groups.

3 Results

3.1 Characterization of HCol and col hydrogels

The cross-linking of HCol hydrogels was schematically shown in Fig. 1A. The adjacent hydroxyl groups (-OH) in hyaluronic acid molecules were oxidized to aldehyde groups (-CHO) by the strong oxidant sodium periodate. The oxidation degree of the prepared OHA was 22% as determined by the hydroxylamine hydrochloride method. Under neutral conditions, the OHA solution could uniformly mix with the Col I solution, and the amino groups (-NH_2) reacted with -CHO to form Schiff base structures, and achieved a certain degree of cross-linking [25]. After gelation at 37 °C, all hydrogels were stable and the pure collagen (Col20) appeared milky white owing to self-assembly, while the cross-linked groups (HCol10 and HCol20) were transparent (Fig. 1B). The FT-IR (Fig. 1C) spectra showed that the infrared absorption of HA remained consistent before and after oxidation, which indicated that the current oxidation degree

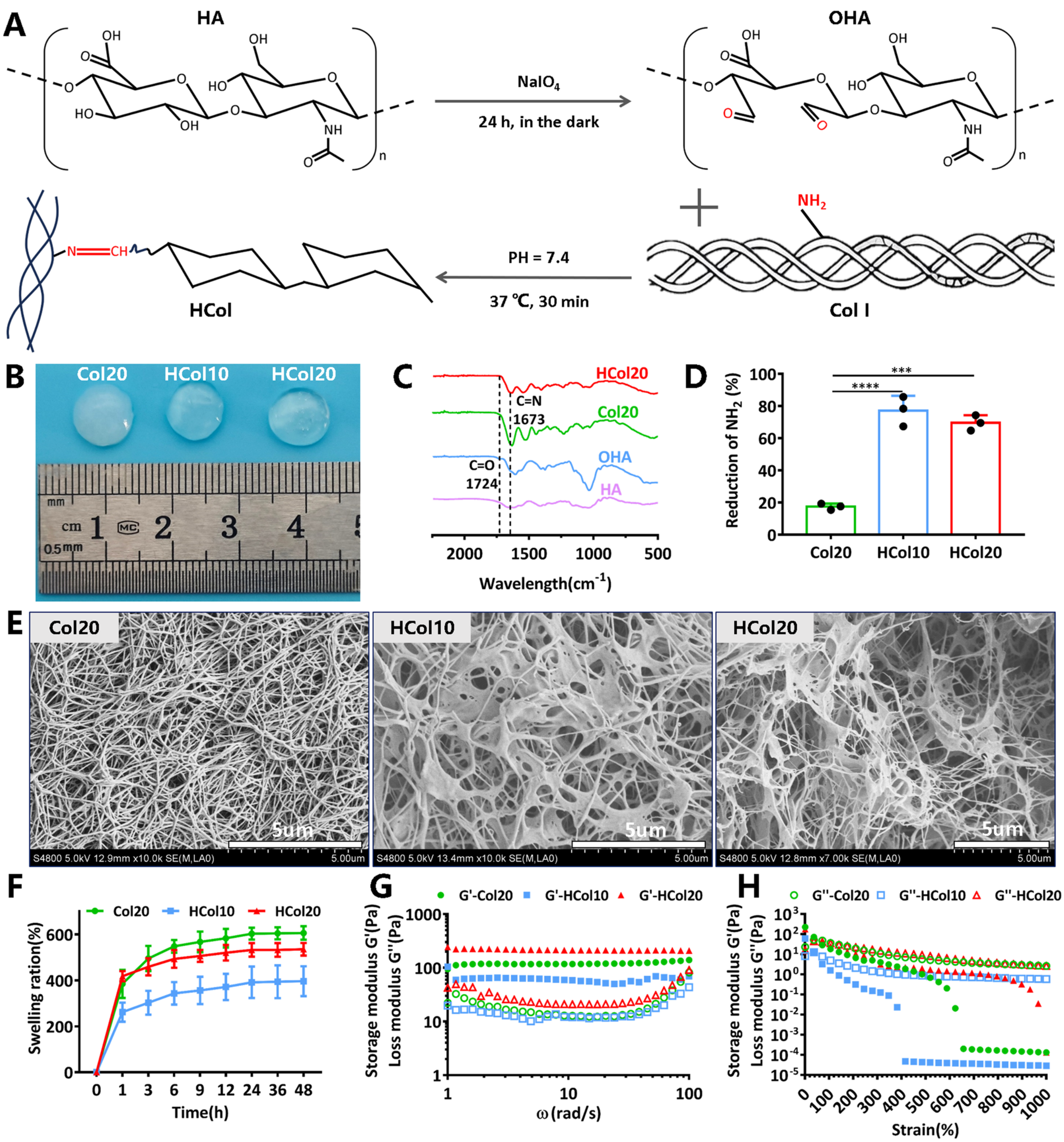

Fig. 1 Formation mechanism and physical properties of HCol and Col hydrogels. **A** Schiff base reaction. **B** Appearance of Col20 and HCol hydrogels. **C** FT-IR spectra of HA, OHA, Col20, and HCol20. **D** The reduction of NH_2 ($n = 3$). **E** The morphology of Col20 and HCol hydrogels evaluated by SEM. **F** Swelling ratio of Col20 and HCol hydrogels in PBS ($n = 3$). **G**-**H** Evaluation of elastic storage modulus G′ and viscous loss modulus G″ by rheology

had no significant impact on the overall molecular structure of HA. The new absorption peak at 1724 cm^{-1} corresponded to the stretching vibration absorption peak of -C=O in the aldehyde group formed after partial ring-opening oxidation of HA [26]. In the infrared spectrum of HCol20, the aldehyde absorption peak at 1724 cm^{-1} nearly disappeared, and a new absorption peak appeared at 1673 cm^{-1}, which was attributed to the stretching vibration peak of the imine group (-C=N-) [27], and indicated the consumption of -CHO in OHA during the formation of gels since -CHO reacted with -NH_2 of Col I in a Schiff base manner. The consumption ratio of -NH_2

measured by the OPA fluorescence method (Fig. 1D) reflected the cross-linking degree of collagen. The formation of Col20 involved no chemical cross-linking, and the slight decrease of -NH_2 content was possibly due to the unavailability of active groups caused by self-assembly and intramolecular folding. By contrast, the -NH_2 consumptions in HCol10 and HCol20 were as high as 70%, with HCol10 showing slightly higher, which meant that an increase in the proportion of OHA to Col I enhanced the degree of cross-linking to some extent. The cross-sectional morphology of the freeze-dried hydrogels shown in Fig. 1E displayed a continuous irregular 3D porous structure with a connection between collagen fibers and sheet-like hyaluronate in cross-linked hydrogels, while only the fibrous network was observed in Col20. The internally irregular pores in the highly cross-linked HCol10 were denser but larger, while those in HCol20 were sparser and smaller in size.

Since the inner structure of hydrogel was a 3D interconnected network, water absorption and swelling behaviors were crucial to hydrogel stability. As the experimental results shown in Fig. 1F, after immersing in PBS for 1 h, the swelling ratio of all hydrogels exceeded 200% and reached swelling equilibrium after 24 h. The initial rapid swelling was mainly due to the unsaturated water absorption and porous structure of the scaffold, while the subsequent slow swelling was related to the dynamic exchange of water throughout the hydrogel network. The swelling ratio of Col20 was the highest from 3 h on, and HCol10 showed the lowest swelling ratio, which also suggested the influence of chemical cross-linking on mechanical properties. By applying a fixed strain amplitude (1%) and temperature (25°C) and varying the frequency of dynamic sweeps, the frequency dependence of G', G" tested over a wide range was shown in Fig. 1G. It presented that the storage modulus of HCol20 was higher than that of Col20 and HCol10, and HCol20 showed good toughness and higher strength. In addition, by applying a constant frequency (10 rad/s) and imposing strain, the relationship between the hydrogel's G', G" and strain were measured. Linear viscoelastic behavior occurred when the strain was less than a critical value, while non-linear behavior occurred when the strain exceeded this value, with G' gradually decreasing below G". From the dynamic strain sweep graph in Fig. 1H, it was observed that within a low strain range, the hydrogel maintained good linear viscoelastic behavior. As the strain increased gradually (100–1000%), the hydrogel showed nonlinear behavior, with a gradual decrease in the storage modulus and a marginal decrease in the loss modulus, indicating structural damage to the hydrogel. The critical point value was highest in HCol20, indicating its superior toughness.

3.2 In vitro cell culture

3.2.1 Cell viability, proliferation and morphology

The live/dead staining images displayed a homogeneous distribution of live cells on the hydrogels (Fig. 2A). Moreover, with increasing culture time, the intensity of green fluorescence steadily increased, and only a few dead cells were detected, indicating that the cells cultured on the hydrogels exhibited good vitality and proliferation. The CCK-8 assay results demonstrated a significant increase in cell number for all groups from 1 to 7 days (Fig. 2C), with the HCol10 group showing the highest proliferation rate, in line with the live/dead staining.

During the initial days of co-culture, the cells exhibited spreading and immediate adhesion to the hydrogels, as evidenced by F-actin and nucleus (blue) staining of the cytoskeleton (Fig. 2A). After 3 days, a full and well-spread morphology was observed. Notably, the actin filaments within the cell nuclei were easily recognizable and displayed normal morphology. The distribution and morphology of the cells observed in the SEM images corresponded to the nucleus and F-actin staining (Fig. 2B). The individual cell spreading areas progressively expanded, and after 7 d, the entire visual field was covered. Similarly, the cell spreading effect of HCol10 was better than that of the other two groups.

3.2.2 Gene expression

The expression of five representative genes, namely Col I and Col IV (which were important components of the extracellular matrix), VEGF and bFGF (which were widely recognized as important factors affecting vascular growth and showed chemotactic effects on fibroblasts), and TGFβ1 (which promoted the transformation of dermal stromal cells into fibroblasts and the proliferation and differentiation of fibroblasts) [28, 29], were determined by RT-PCR and the results were shown in Fig. 2D-H. The results indicated that all hydrogels overall promoted the expression of the 5 genes. Specifically, the expression of Col I and Col IV genes in Col20 and HCol10 were up-regulated at 7 d, and the expression was promoted at 14 d while Col20 showed the most significant promoting effect (Fig. 2D-E). At 7 d, the VEGF expression was significantly promoted in three hydrogels, while the expression in Col20 was down-regulated at 14 d; meanwhile, the VEGF expression in HCol10 and HCol20 still be up-regulated but with reduced promotion effects (Fig. 2F). Similarly, the three hydrogels promoted the expression of bFGF and TGFβ1 at 7 d, with the promoting effect of both growth factors reduced at 14 d except the bFGF expression in HCol20 (Fig. 2G-H).

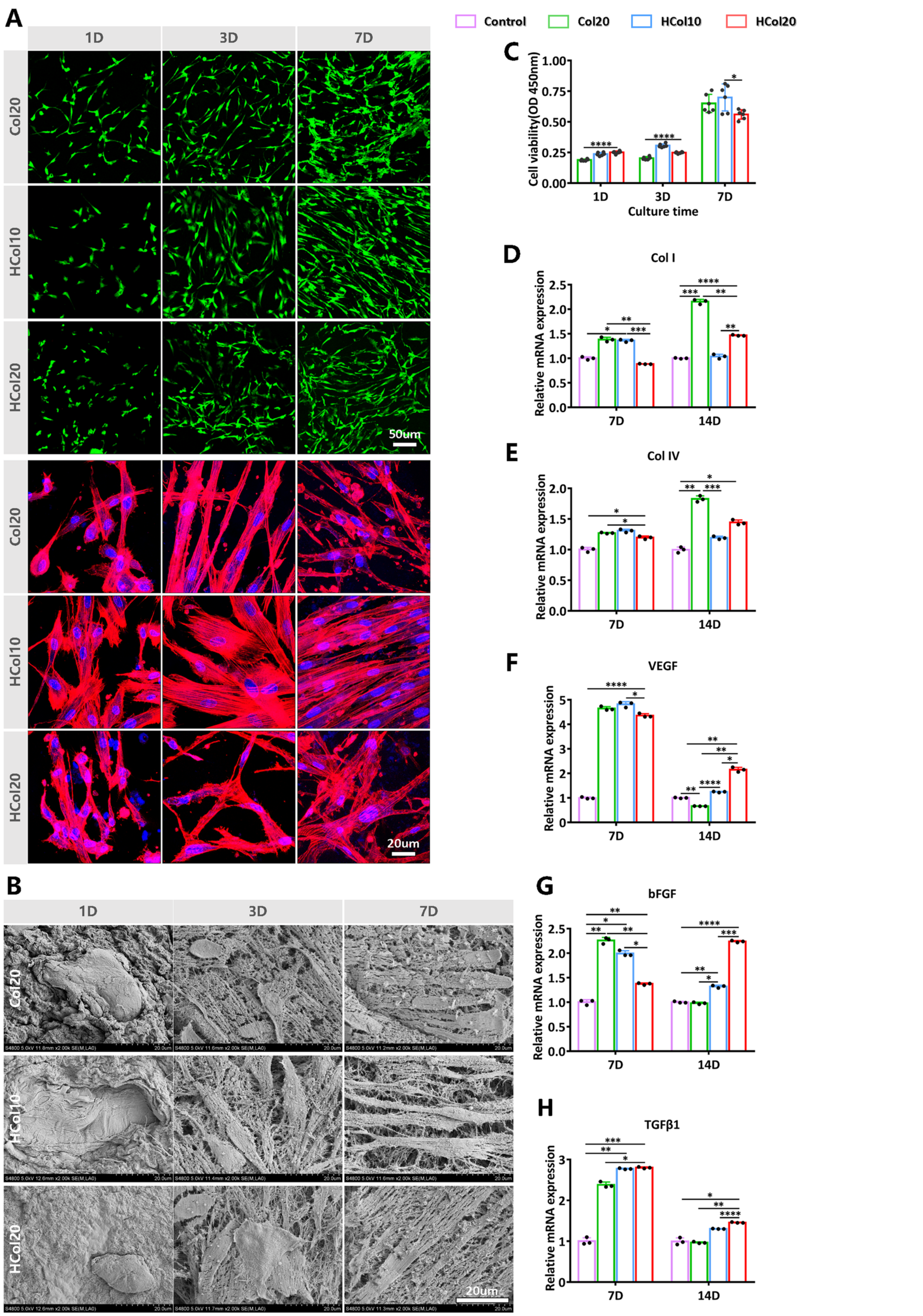

Fig. 2 Viability, proliferation and morphology of HSFs cultured on HCol hydrogels. **A**-**B** Viability and morphology of HSFs on HCol hydrogels evaluated by confocal microscope and SEM (FDA/PI staining; green: live cells; red: dead cells, F-actin fluorescence staining). **C** Proliferation of HSFs on HCol hydrogels evaluated by CCK-8 assay ($n = 6$). **D**-**H** Expression of the Col I, Col IV, VEGF, bFGF, and TGFβ1 genes at 7 and 14 days. Every outcome was normalized based on the expression of GAPDH levels ($n = 6$)

3.3 In vivo animal study

3.3.1 General observation

As previously described, three material groups together with a commercial product were injected subcutaneously with 200 μL per site in adult SD rats. It was easy to inject these materials into the subcutaneous area, which was consistent with the rheological yielding behavior observed during the transition from solid to liquid-like properties under high shear. Also, the shape of all injected fillers could be easily adjusted and maintained, and the volume increase at the injection site could be clearly observed (Fig. 3B).

3.3.2 MRI analysis

The in vivo volume retention of the injected implants over time was quantified using magnetic resonance imaging (MRI) and the results were shown in Fig. 3C. The image acquisition was conducted post-operative 1 d and monthly afterwards, and the retained volume of the implant was further calculated after the manual depiction of the implant contour. The volume retentions of different groups were plotted over time in Fig. 3D. Firstly, it was found that the volume of implants varied between collagen and hyaluronate hydrogels at 1d post-injection. To be specific, collagen-based hydrogels were significantly contracted to a smaller volume than the injected volume (200 μL), while the volume of implanted CHA was dramatically increased after 1 d. During the 3 months observation course, collagen hydrogels degraded at a faster rate while the CHA was largely reserved with a volume retention of 77% ± 5%. However, collagen-based hydrogels still could be observed in vivo 3 months post-injection, even though both Col20 and HCol10 were degraded to only 13% ± 4%. Among the collagen hydrogels, the volume retention of HCol20 was the largest and around 31% ± 4% after 3 months.

3.3.3 Histological examination

The animals were sacrificed at the defined time to collect the implants and adjacent tissue to have visual inspection and histological evaluation. HE staining results showed that the four hydrogels showed good biocompatibility with no significant inflammation or granulation tissue after implantation (Fig. 4A). 1 month after the implantation, no obvious implant contour and few infiltrated cells were observed in collagen hydrogels, while there was a clear boundary between the filler and tissue and only a small number of cells aggregated around but not migrated into the CHA. By the second and third months, collagen-based hydrogels were gradually hard to distinguish from the adjacent tissue. The structure of collagen fibers in Col20 and HCol20 was clear and dense at 2 M

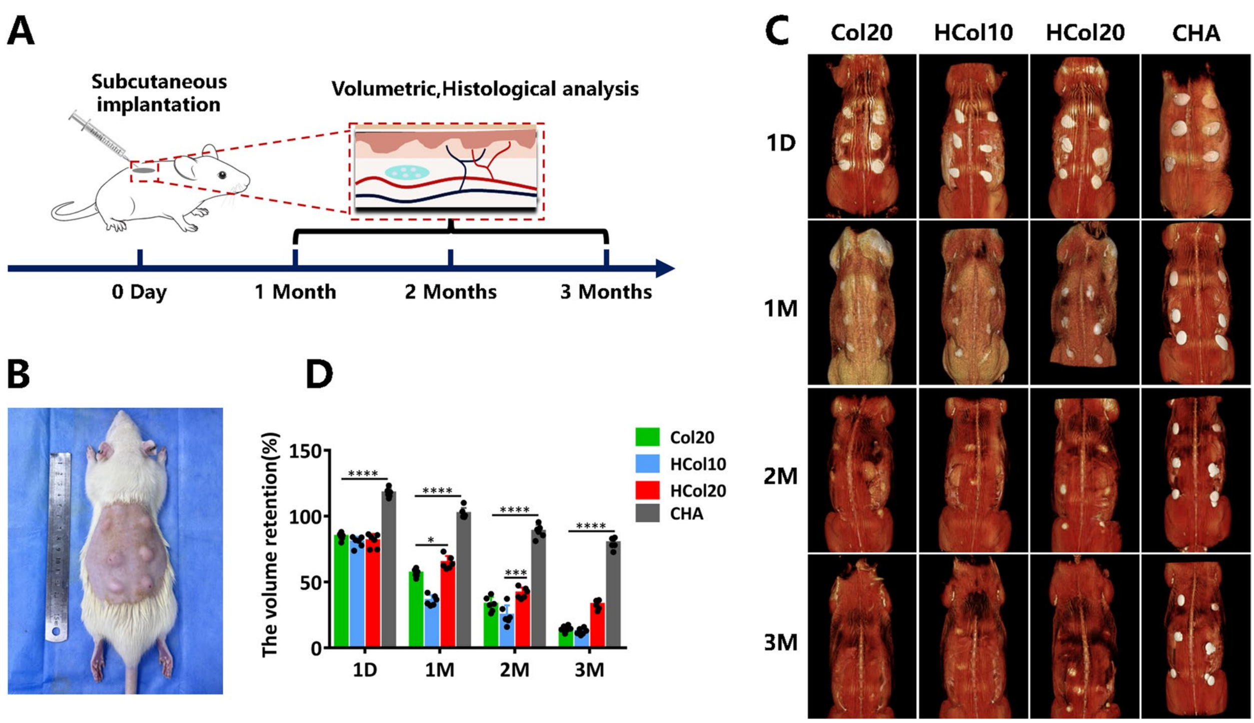

Fig. 3 Animal experiment cycle and detection of hydrogel retention volume in vivo. **A** Construction of subcutaneous implantation model and sampling period. **B** Back state of rats immediately after implantation. **C** Representative MRI images of rats scanned at 1, 2 and 3 months after the injection procedure. **D** Results of the volume retention during the study ($n = 6$)

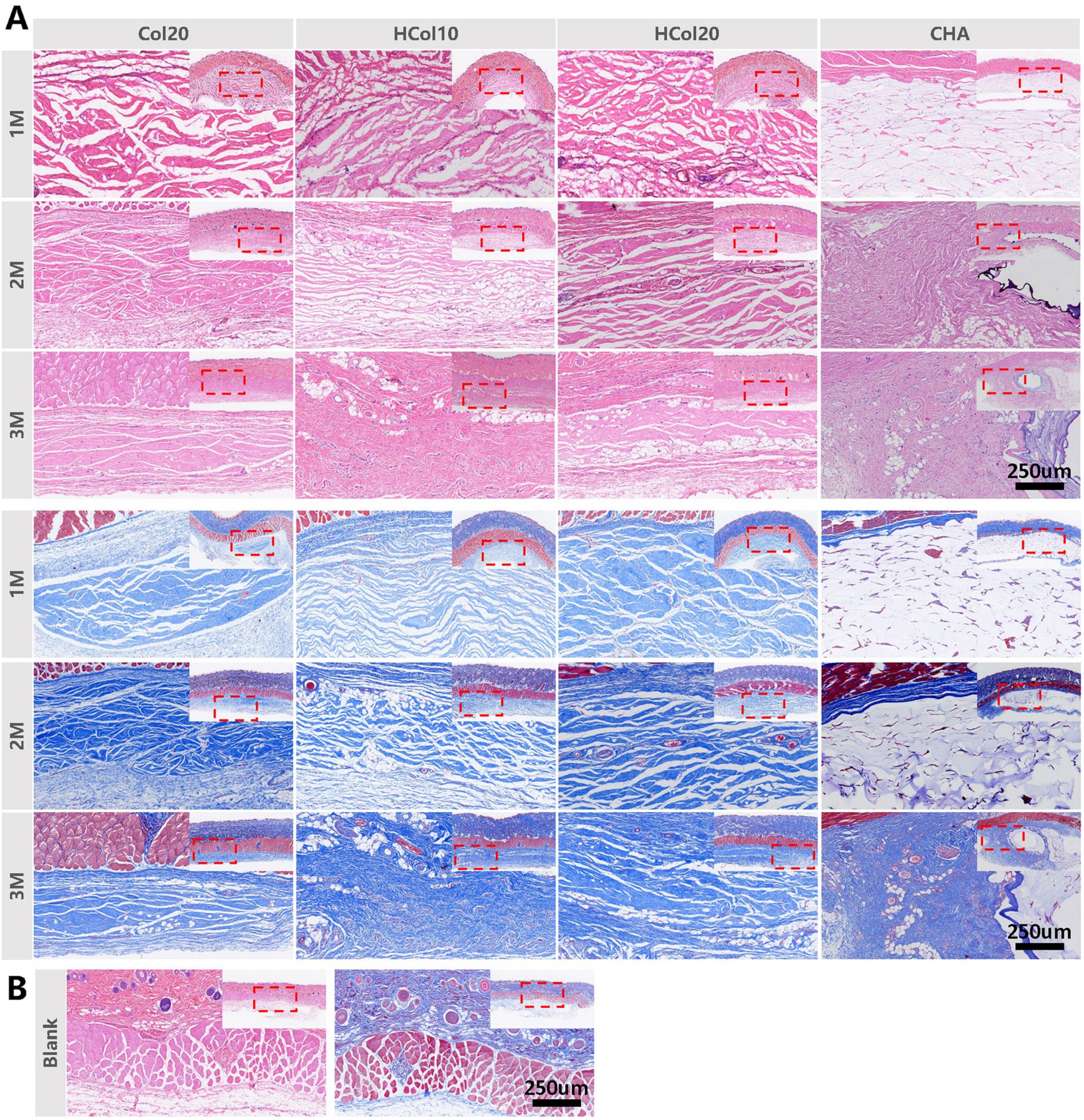

Fig. 4 Histological evaluation of the hydrogels after implantation. **A** Identification of inflammation and foreign body reaction by hematoxylin and eosin staining, and identification of collagen production by Masson's trichrome staining at 1, 2 and 3 months. **B** The HE and Masson staining of blank control

but appeared loosely arranged at 3 M. In contrast, collagen fibers in HCol10 showed lower density at 2 M and became denser and randomly arranged at 3 M. Meanwhile, the CHA still could be easily found in the tissue which was consistent with the result acquired from the MRI test. Cells around were dense and infiltrated inward, with collagen fibers only generated around the CHA. Notably, vascularization was observed in the hydrogels at the same time, with the most significant vascularization seen in HCol10 and HCol20. Collagen deposition could be further confirmed by Masson's trichrome staining, in which the darker blue indicated more collagen synthesized. The staining results indicated that HCol10 and HCol20 were associated with greater collagen synthesis compared to Col20 and CHA. All four hydrogels showed no obvious collagen synthesis at 1 M, which was consistent with the HE results and demonstrated cytocompatibility. Collagen deposition appeared around and within collagen-based hydrogels at 2 M. The Col20 showed the most significant collagen synthesis, followed by HCol20, and HCol10 exhibited relatively sparse collagen fibers, while CHA only exhibited peripheral collagen deposition. Finally, the collagen bundles in Col20 were sparse and thin at 3 M, while HCol10 and HCol20 displayed significant collagen synthesis, with collagen fibers in HCol20 arranged in bundles, and the collagen content and density markedly increased in HCol10. Similarly, only the density of surrounding collagen fibers increased for CHA at 3 M.

3.3.4 SHG signal analysis

Collagen fibers could be visualized in situ by second-harmonic generation (SHG) imaging, which was a multi-photon microscopic observation without sample staining [30]. SHG signals were utilized to characterize the microstructure of collagen tissue surrounding and inside the implants, and the SHG signal intensity could indicate the relative collagen content. The original SHG signal images collected by the two-photon microscope were shown in Fig. 5A and B-D displayed the statistical results of signal intensity. The results showed that there was almost no signal inside the hydrogels at 1 M, only weak SHG signals were detected in the surrounding area, and the collagen mostly appeared as thin fibers. Consistent with Masson staining results, the results indicated a relatively low collagen content was deposited at 1 M. We suggested that the observed collagen was type III collagen. On the contrary, there was almost no signal could be found in CHA, but the signal intensity around the implant was obviously stronger and denser which implicated the hyperplasia of capsule. At 2 M post-injection, seldom SHG signals were detected inside the CHA hydrogel, while the

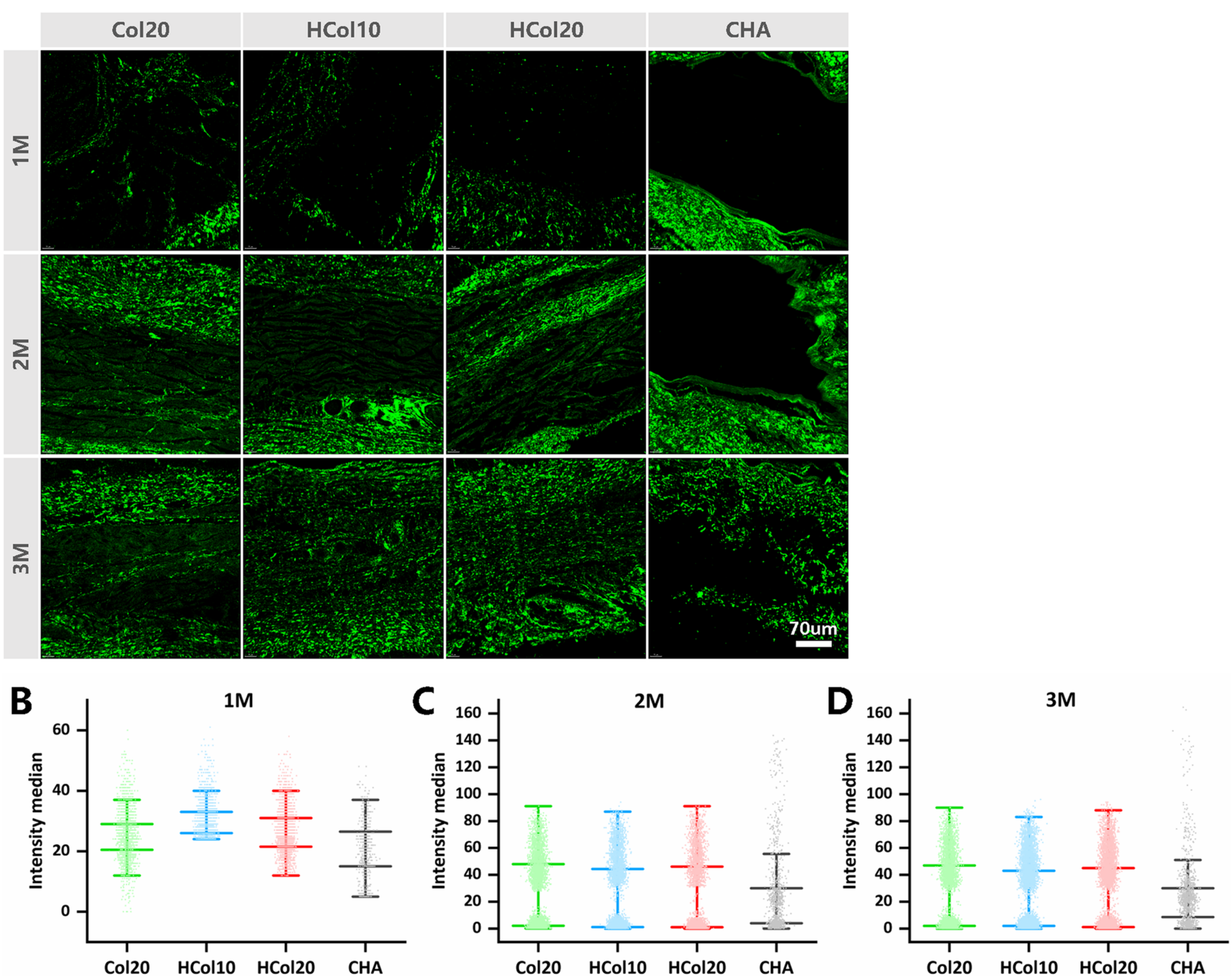

Fig. 5 The changes of the SHG signals at 1, 2 and 3 months for each group (Col20, HCol10, HCol20 and CHA). **A** The SHG signal images collected by the two-photon microscope. **B**-**D** the statistical results of SHG signal intensity

positive signals around the filler were still strong which indicated an increase in collagen content. The signals collected from collagen hydrogels intensified at 2 M, especially inside the hydrogels. More importantly, the bundled collagen fibers were apparently visible in the hydrogels, which suggested a biomimetic reconstruction of the extracellular matrix in the tissue. At the final observation time point, slight signals could be found in the internal CHA hydrogel, with a dominant area without positive signals. The SHG signal strength and distribution in Col20 showed no significant changes compared to that observed at 2 M. However, the internal SHG signals of HCol10 and HCol20 not only intensified but also presented a similar morphology as the extracellular matrix in adjacent tissue, indicating a matured and remodeled dermal matrix was formed.

4 Discussion

Dermal fillers for facial rejuvenation should possess several characteristics to ensure biosafety and efficacy after being implanted, including biocompatibility, non-immunogenicity, biodegradability, in vivo stability, and the ability to promote collagen regeneration [31–34]. Collagen enjoys the advantages as the starting material of implantable medical devices for its excellent biological functions [35–38], but its deficiencies also limit further application such as weak mechanical properties, prone to degradation, and challenging to preserve [39, 40]. The advances in the preparation and modification of collagen-based biomaterials could enhance their suitability for diverse applications [40, 41]. The presence of HA in a collagen matrix has been shown to enhance cell division in human fibroblasts by their passage through cell cycles [42]. HA could also induce cell aggregation, proliferation, and angiogenesis [43, 44], and regulate the process of inflammation promoting tissue regeneration [45]. In previous research to prepare various types of composites such as non-crosslinked [46], crosslinked [47], chemically modified [48], and interconnected composites [49], hyaluronic acid had demonstrated successful integration with soft tissue implants. Thus, it could be a possible strategy to prepare composite hydrogels based on collagen and hyaluronic acid with satisfied mechanical and biological properties for facial implantation.

In this study, an injectable hydrogel based on hyaluronic acid and type I collagen was prepared and evaluated for volume maintenance and tissue regeneration. Primarily, HCol hydrogels offered a stable injectable dermal filler formed in situ through a straightforward preparation process. Additionally, HCol hydrogels played a significant role in maintaining optimal biodegradability and biocompatibility. Eventually, these hydrogels facilitated fibroblast migration, vascularization, and collagen deposition, thereby enhancing tissue durability and supporting skin regeneration.

As reported by Allemann et al. [50], the addition of HA influenced the density and pore size of HCol hydrogels. We observed that the hydrogel pores were more irregular and fibrotic with the increasing crosslinking degree [17, 27]. In addition, with the increase in collagen concentration, the pore size of collagen-based hydrogels became smaller [51]. The molecular weight of macromolecular monomers, the concentration of macromolecular monomers, the concentration of crosslinking agents, and the degree of crosslinking can affect the swelling rate of crosslinked composite materials [52]. Usually, a higher degree of crosslinking leads to lower water absorption [53]. The lower swelling rate of HCol10 was related to its larger pore size and higher crosslinking density. The injection force of the dermal filler was affected by the rheological and physiochemical properties of the filler composite, which included viscosity, particle size, crosslinking density, and polymer concentration [54, 55]. HCol hydrogels exhibited no significant differences in morphology compared to Col20, but their rheological properties were confirmed to be different. The storage modulus and the loss modulus increased with increasing frequency, indicating physical entanglement in the reversible dynamic chemical crosslinking network [54]. However, the hardness and elasticity of crosslinked gels were not always superior to pure collagen gels. The reduced solidity of HCol10 primarily stemmed from a lower concentration of solid content and the diminished self-assembly of collagen post-chemical crosslinking. The rigidity of HCol20 was hard with the increase of solid content and certain chemical crosslinking. Furthermore, all hydrogels exhibited yielding behavior characterized by a transition to a liquid-like state, as indicated by the intersection and surpassing of G' curves by G" curves under high shear deformation. This viscoelastic yielding mechanism, inherent to collagen hydrogels, enabled them to maintain structural integrity under static conditions while remaining injectable [56]. The use of highly reactive crosslinkers like divinyl sulfate (DVS), 1,4-butanediol diglycidyl ether (BDDE), and 1,2,7,8-diepoxoctane (DEO) could produce harder HA fillers [57, 58]. However, the increased compression of these fillers and fragments of gel after injection may lead to a higher risk of complications such as vascular embolism [59, 60]. Oxidative modification of HA combined with collagen crosslinking, produced HCol fillers that were relatively soft and easy to inject, while still maintaining stability. This approach could reduce the risk of vascular embolism.

Biomaterials intended for injection or implantation must undergo comprehensive short-term and long-term studies to evaluate potential acute and delayed cytotoxic effects [27]. In vitro cell culture showed that HCol10 promoted cell proliferation and spread better than the pure collagen group, while HCol20 hydrogel had no obvious advantage. Generally, the internal three-dimensional structure, including pore size and porosity, has been proven to regulate cell behavior [61]. Suitable pore sizes were necessary for tissue formation to facilitate the diffusion of nutrients, oxygen, and waste products to and from cells [27]. The HCol10 showed the best overall effect in promoting HSF proliferation, with larger micropores that were profit to cell growth. RT-qPCR results suggested that HCol hydrogels promoted the expression of extracellular matrix and angiogenesis. The differentiation of cells in the hydrogel was affected by the swelling ratio [62], which may be related to the diffusion of signal molecules and nutrients in the hydrogel. In addition, with the increase of collagen concentration, the pore size of collagen-based hydrogel was smaller, which was not suitable for cell inoculation and survival [51]. Compared with HCol20 and Col20, HCol10 had the best effect on cell proliferation, spreading and gene expression, which may be due to the lower concentration and softer, which was conducive to cell adhesion on the surface and growth. Thus, the HCol hydrogels developed by appropriate components and moderate cross-linking not only provided appropriate adhesion sites and chemical microenvironment but also supported cells with suitable inner structure and mechanical cues to modulate cell phenotypes.

Furthermore, the as-obtained collagen hydrogels were in vivo evaluated with subcutaneous models, using commercial hyaluronic acid sodium gel CHA as the control. Based on histocompatibility assessment requirements of foreign materials implanted in vivo, biocompatible biomaterials should show less intense immune responses or no material rejection [27]. The research that investigated hyaluronic acid hydrogels prepared by a similar pattern was noted to degrade within the range of 10–36 weeks, which was comparable to our results [47]. The HCol hydrogels combined injectability with retained volume for at least 3 months. Increasing concentration and crosslinking modification might further improve hydrogel retention time and volume in vivo. The MRI results indicated that chemical crosslinking enhanced the enzymatic hydrolysis resistance of HCol hydrogel in vivo. The continuous compressive forces exerted by skin tension and external pressure in vivo [63] led to the volume contraction of collagen-based hydrogels during the initial implantation period. Despite Col20 displaying higher elastic modulus in vitro, it exhibited weak toughness, unstable structure under external forces and enzymatic hydrolysis in vivo [54]. Nevertheless, commercially available CHA demonstrated enhanced stability in vivo, leading to a more pronounced tissue volumizing effect post-injection, with degradation initiated gradually after a month. The interaction between collagen and HA with fibroblast surface receptors was pivotal for extracellular matrix remodeling, including collagen deposition and angiogenesis [64, 65]. Collagen featured binding sites for the β1 subunit, as well as the α1, α2, α10, and α11 subunits, which induced proliferation of keratinocytes, fibroblasts, and myofibroblasts [21, 64]. HA, through the CD44 molecule, effectively promoted cell signaling, cytokine release, extracellular matrix deposition, and angiogenesis [60, 66, 67]. Histological staining results showed an increase in fibroblast numbers post-injection, possibly due to fibroblasts attaching to the hydrogel via fibronectin and CD44. The increase in fibroblasts was particularly evident in HCol hydrogels, and this effect persisted for three months. At 3 M, purple staining indicated HCol hydrogel degradation and cell uptake of partly degraded material, in line with observations from related research [63]. SHG signal in biological tissues was highly sensitive to the changes in tissue microstructure, with collagen content closely linked to signal strength due to collagen's strong second-order nonlinear polarizability and non-centrosymmetry [30, 68–71]. Analysis of SHG signals was in line with the Masson staining findings, demonstrating the superior collagen regeneration promotion effect of HCol hydrogel compared to CHA. Previous studies indicated that the volume of injected hydrogel, degradation time, and crosslinking degree of the hydrogel could affect fibroblast proliferation and extracellular matrix secretion [64]. In a study, injection of biphasic hyaluronic acid led to increased collagen deposition and angiogenesis around the filler, which lasted up to 12 weeks post-injection [72]. In our study, HCol hydrogels exhibited good compatibility with surrounding tissues and significant stimulation of collagen and angiogenesis. The process of angiogenesis in hydrogels provided a framework for tissue filling materials as they gradually degrade [72]. On the other hand, CHA maintained longer residence time in vivo, and had distinct boundaries with surrounding tissues, but only showed an increase in collagen content around the filler at 3 M. Overall, HCol hydrogels exhibited excellent biocompatibility, facilitating vascular growth and collagen regeneration.

5 Conclusion

In the study, an injectable HCol hydrogel was formed by the Schiff base reaction between collagen type I and oxidized hyaluronic acid, avoiding the chemical crosslinking of high molecule weight HA which might cause various side effects after implantation. Characterization of physicochemical properties and in vitro and in vivo biocompatibility experiments demonstrated that the hydrogel network was stable, conducive to cell adhesion and spreading, and promoted vascular ingrowth and collagen regeneration. According to current results, the HCol10 was the most advantageous and the fibrous network could most effectively support the attachment of the cells. The implantation in vivo showed good vascularization and connective tissue formation while maintaining shape and integrity. In summary, the HCol hydrogel could accelerate skin regeneration with enhanced stability and excellent biocompatibility, which appeared to have beneficial properties for use as an implant in skin soft tissue.

Abbreviations

Col	Collagen
Col I	Type I collagen
Col20	Type I collagen hydrogel, 20 mg/ml
HA	Hyaluronic acid
HCol	Hydrogel composed of HA and Col I
HCol10	Hydrogel composed of HA and Col I (10 mg/ml, final concentration of Col I)
HCol20	Hydrogel composed of HA and Col I (20 mg/ml, final concentration of Col I)
CHA	Cross-linked Sodium Hyaluronate Gel (product control)
OHA	Derivative of oxidized hyaluronic acid
PMMA	Poly-methyl methacrylate
PLLA	Poly-L-lactic acid
CaHA	Calcium hydroxyapatite
BDDE	1,4-butanediol diglycidyl ether
HSF	Human skin fibroblast cell
FBS	Fetal bovine serum
FDA	Fluorescein diacetate
PI	Propidium iodide
DAPI	4′6-diamidino-2-phenylindole
OPA	O-phthalaldehyde
DMEM	Dulbecco's Modified Eagle Medium
CCK-8	Cell Counting KIT-8
Col IV	Type IV collagen
VEGF	Vascular endothelial growth factor
bFGF	Basic fibroblast growth factor
TGFβ1	Transforming growth factor beta
cDNA	Complementary DNA
MRI	Magnetic resonance images
SHG	Second harmonic generation
DVS	divinyl sulfate
DEO	1,2,7,8-diepoxoctane

Acknowledgements
We would like to thank Ping Liao from the Anesthesia and Critical Care Research Laboratory - Optoelectronic Platform at West China Hospital of Sichuan University, for her technical assistance in SHG.

Authors' contributions
Lu Song: Writing – original draft, Validation, Methodology, Investigation, Formal analysis, Data curation, Conceptualization. He Qie: Investigation, Formal analysis. Zhiru Chen: Visualization, Investigation. Jing Wang: Visualization, Investigation. Yang Xu: Investigation, Formal analysis. Zhanhong Liu: Investigation, Formal analysis. Shuo Liu: Visualization, Investigation. Zhiyuan Wang: Visualization, Investigation. Xiangdong Zhu: Validation, Supervision. Kai Zhang: Supervision, Resources, Project administration. Hai Lin: Writing – review & editing, Validation, Supervision, Resources, Funding acquisition, Conceptualization. Xingdong Zhang: Project administration, Supervision.

Funding
This work was financially supported by the National Natural Science Foundation of China (32371399), the National Key Research and Development Program of China (2022YFC2409803) and the Key Research and Development Program of Sichuan Province (23ZDYF2553).

Availability of data and materials
All the data supporting the findings of this study are available within the article.

Declarations

Ethics approval and consent to participate
The animal study was approved by the Experimental Animals Ethics Committee of Sichuan University (No. K2023011). All the animals were purchased from Chengdu Dossy Experimental Animals Co., Ltd. The animal experiment guidance from the ethical committee and the guide for care and use of laboratory animals of Sichuan University were followed during the whole experiment course.

Consent for publication
All authors have given approval to the final version of the manuscript.

Competing interests
Hai Lin serves as the Associate Editor-in-Chief of Collagen and Leather, and he was not involved in the editorial review, or the decision to publish this article. All authors declare that there are no competing interests.

Author details
[1]National Engineering Research Center for Biomaterials, College of Biomedical Engineering, Sichuan University, Chengdu, Sichuan 610064, China. [2]State Key Laboratory of Oral Diseases, National Center for Stomatology, National Clinical Research Center for Oral Diseases, Med-X Center for Materials, West China Hospital of Stomatology, Sichuan University, Chengdu, Sichuan 610041, China.

Received: 6 April 2024 Revised: 29 April 2024 Accepted: 10 May 2024
Published online: 01 June 2024

References

1. Fallacara A, Manfredini S, Durini E, et al. Hyaluronic acid fillers in soft tissue regeneration. Facial Plast Surg. 2017;33(01):087–96.
2. Kim JH, Kwon TR, Lee SE, et al. Comparative evaluation of the effectiveness of novel hyaluronic acid-polynucleotide complex dermal filler. Sci Rep. 2020;10(1):5127.
3. Ballin AC, Brandt FS, Cazzaniga A. Dermal fillers: an update. Am J Clin Dermatol. 2015;16:271–83.
4. Jones DH. Semipermanent and permanent injectable fillers. Dermatol Clin. 2009;27(4):433–44, vi.
5. Kulichova D, Borovaya A, Ruzicka T, et al. Understanding the safety and tolerability of facial filling therapeutics. Exp Opin Drug Saf. 2014;13(9):1215–26.
6. Funt D, Pavicic T. Dermal fillers in aesthetics: an overview of adverse events and treatment approaches. Plast Aesthetic Nurs. 2015;35(1):13–32.
7. Egbert M, Ruetze M, Sattler M, et al. The matricellular protein periostin contributes to proper collagen function and is downregulated during skin aging. J Dermatol Sci. 2014;73(1):40–8.
8. Lee DH, Oh JH, Chung JH. Glycosaminoglycan and proteoglycan in skin aging. J Dermatol Sci. 2016;83(3):174–81.
9. Fitzgerald R, Graivier MH, Kane M, et al. Update on facial aging. Aesthetic Surg J. 2010;30(1Supplement):S11–24.
10. Dermatologic surgery: step by step. Wiley. 2012. https://doi.org/10.1002/9781118412633.ch54.
11. Danny Vleggaar MD. Dermatological implications of skeletal. aging: afocus on supraperiosteal volumization for perioral rejuvenation. J Drugs Dermatol. 2008;7(3):210.
12. Fisher GJ, Varani J, Voorhees JJ. Looking older: fibroblast collapse and therapeutic implication. Arch Dermatol. 2008;144(5):666–72.
13. Man MQ, Xin SJ, Song SP, et al. Variation of skin surface pH, sebum content and stratum corneum hydration with age and gender in a large Chinese population. Skin Pharmacol Physiol. 2009;22(4):190–9.

14. Necas J, Bartosikova L, Brauner P, et al. Hyaluronic acid (hyaluronan): a review. Vet Med. 2008;53(8):397–411.
15. Lam J, Truong NF, Segura T. Design of cell-matrix interactions in hyaluronic acid hydrogel scaffold. Acta Biomater. 2014;10(4):1571–80.
16. Salti G, Fundarò SP. Evaluation of the rheologic and physicochemical properties of a novel hyaluronic acid filler range with excellent three-dimensional reticulation (XTR™) technology. Polymers. 2020;12(8):1644.
17. Park SN, Lee HJ, Lee KH, et al. Biological characterization of EDC-crosslinked collagen–hyaluronic acid matrix in dermal tissue restoration. Biomaterials. 2003;24(9):1631–41.
18. Lu Y, Kang W, Yu Y, et al. et al. Antibacterial and antioxidant bifunctional hydrogel based on hyaluronic acid complex MoS2-dithiothreitol nanozyme for treatment of infected wounds. Regen Biomater. 2024;11:rbae025.
19. Fidalgo J, Deglesne PA, Arroyo R, et al. Detection of a new reaction by-product in BDDE cross-linked autoclaved hyaluronic acid hydrogels by LC–MS analysis. Med Devices: Evid Res. 2018;11:367–76.
20. Keizers PHJ, Vanhee C, van den Elzen EMW, et al. A high crosslinking grade of hyaluronic acid found in a dermal filler causing adverse effects. J Pharm Biomed Anal. 2018;159:173–8.
21. Ye X, et al. Preparation and properties of oxidized Hyaluronic Acid / Polyacryloyl Hydrazide Hydrogel. Fine Chemicals. 2018;35(4):591–6.
22. Wang Q, et al. Determination of aldehyde group concentration on oxidized sodium alginate by hydroxylamine hydrochloride-potentiometric titratio. Chin J Anal Lab. 2008;27(S1):4.
23. Nielsen PM, Petersen D, Dambmann C. Improved method for determining food protein degree of hydrolysis. John Wiley & Sons, Ltd. 2001;(5). https://doi.org/10.1111/J.1365-2621.2001.TB04614.X.
24. Chen Y, et al. Determination of the isolated amino acid in ginkgo seed by fluorophotometry. Mod Food Sci Technol. 2003;19(002):87–9.
25. Hermanson GT. Chapter 25 - modification with synthetic polymer. Elsevier Inc.; 2008. https://doi.org/10.1016/B978-0-12-370501-3.00025-4.
26. Liu S, Liu X, Ren Y, et al. Mussel-inspired dual-cross-linking hyaluronic acid/ε-polylysine hydrogel with self-healing and antibacterial properties for wound healing. ACS Appl Mater Interfaces. 2020;12(25):27876–88.
27. Ma X, Deng J, Du Y, et al. A novel chitosan–collagen-based hydrogel for use as a dermal filler: initial in vitro and in vivo investigations. J Mater Chem B. 2014;2(18):2749–63.
28. Ray S, Ju X, Sun H, et al. The IL-6 trans-signaling-STAT3 pathway mediates ECM and cellular proliferation in fibroblasts from hypertrophic scar. J Invest Dermatol. 2013;133(5):1212–20.
29. Subramaniam N, Petrik JJ, Vickaryous MK, VEGF. FGF-2 and TGF β expression in the normal and regenerating epidermis of geckos: implications for epidermal homeostasis and wound healing in reptiles. J Anat. 2018;232(5):768–82.
30. Jiang X, Zhong J, Liu Y, et al. Two-photon fluorescence and second-harmonic generation imaging of collagen in human tissue based on multiphoton microscopy. Scanning. 2011;33(1):53–6.
31. Ji DY, Kuo TF, Wu HD, et al. A novel injectable chitosan/polyglutamate polyelectrolyte complex hydrogel with hydroxyapatite for soft-tissue augmentation. Carbohydr Polym. 2012;89(4):1123–30.
32. Choi WI, Hwang Y, Sahu A, et al. An injectable and physical levan-based hydrogel as a dermal filler for soft tissue augmentation. Biomaterials Sci. 2018;6(10):2627–38.
33. Cho KH, Uthaman S, Park IK, et al. Injectable biomaterials in plastic and reconstructive surgery: a review of the current status. Tissue Eng Regen Med. 2018;15:559–74.
34. Skrzypek E, Górnicka B, Skrzypek DM, et al. Granuloma as a complication of polycaprolactone-based dermal filler injection: ultrasound and histopathology studies. J Cosmet Laser Ther. 2019;21(2):65–8.
35. Xiaoyue Y, Haiping Z, Yiliang M, et al. Recent strategies of collagen-based biomaterials for cartilage repair: from structure cognition to function endowment. Coll Leather. 2022;4:11.
36. Xiaotong C, Tao Y, Qunshou K, et al. Functional non-glutaraldehyde treated porcine pericardium for anti-coagulation, anti-calcification, and endothelial proliferation bioprosthetic heart valves. Coll Leather. 2022;4:23.
37. Jiayi Z, Zhulian L, Yaping Z, Gonggong L, et al. Advanced application of collagen-based biomaterials in tissue repair and restoration. Coll Leather. 2022;4:30.
38. Qijue C, Ying P, Keyong T, et al. Structure, extraction, processing, and applications of collagen as an ideal component for biomaterials - a review. Coll Leather. 2023;5:20.
39. Mathew-Steiner SS, Roy S, Sen CK. Collagen in wound healing. Bioengineering. 2021;8(5):63.
40. Eyre DR, Wu JJ. Collagen cross-links. Collagen: primer in structure, processing and assembly. 2005. p. 207–29.
41. Huang Y, Sun M, Lu Z, et al. Role of integrin ß1 and tenascin C mediate TGF-SMAD2/3 signaling in chondrogenic differentiation of BMSCs induced by Type I Collagen Hydrogel. Regen Biomater. 2024;11:rbae017.
42. Greco RM, Iocono JA, Ehrlich HP. Hyaluronic acid stimulates human fibroblast proliferation within a collagen matrix. J Cell Physiol. 1998;177(3):465–73.
43. Turley EA, Noble PW, Bourguignon LYW. Signaling properties of hyaluronan receptors. J Biol Chem. 2002;277(7):4589–92.
44. Jooybar E, Abdekhodaie MJ, Alvi M, et al. An injectable platelet lysate-hyaluronic acid hydrogel supports cellular activities and induces chondrogenesis of encapsulated mesenchymal stem cells. Acta Biomater. 2019;83:233–44.
45. Suner SS, Demirci S, Yetiskin B, et al. Cryogel composites based on hyaluronic acid and halloysite nanotubes as scaffold for tissue engineering. Int J Biol Macromol. 2019;130:627–35.
46. Okabe K, Yamada Y, Ito K, et al. Injectable soft-tissue augmentation by tissue engineering and regenerative medicine with human mesenchymal stromal cells, platelet-rich plasma and hyaluronic acid scaffolds. Cytotherapy. 2009;11(3):307–16.
47. Yang R, Tan L, Cen L, et al. An injectable scaffold based on crosslinked hyaluronic acid gel for tissue regeneration. RSC Adv. 2016;6(20):16838–50.
48. Yang C, Wang X, Yao X, et al. Hyaluronic acid nanogels with enzyme-sensitive cross-linking group for drug delivery. J Controlled Release. 2015;205:206–17.
49. Park SH, Cho H, Gil ES, et al. Silk-fibrin/hyaluronic acid composite gels for nucleus pulposus tissue regeneration. Tissue Eng Part A. 2011;17(23–24):2999–3009.
50. Allemann F, Mizuno S, Eid K, et al. Effects of hyaluronan on engineered articular cartilage extracellular matrix gene expression in 3-dimensional collagen scaffolds. J Biomed Mater Res. 2001;55(1):13–9.
51. Zhang Y, Wang Y, Li Y, et al. Application of collagen-based hydrogel in skin wound healing. Gels. 2023;9(3):185.
52. Zhang L, Li K, Xiao W, Zheng L, et al. Preparation of collagen–chondroitin sulfate–hyaluronic acid hybrid hydrogel scaffolds and cell compatibility in vitro. Carbohydr Polym. 2011;84(1):118–25.
53. Ghosh K, Shu XZ, Mou R, et al. Rheological characterization of in situ cross-linkable hyaluronan hydrogels. Biomacromolecules. 2005;6(5):2857–65.
54. Yang R, Liu X, Ren Y, et al. Injectable adaptive self-healing hyaluronic acid/poly (γ-glutamic acid) hydrogel for cutaneous wound healing. Acta Biomater. 2021;127:102–15.
55. Tian Z, Liu W, Li G. The microstructure and stability of collagen hydrogel cross-linked by glutaraldehyde. Polym Degrad Stab. 2016;130:264–70.
56. Béduer A, Genta M, Kunz N, et al. Design of an elastic porous injectable biomaterial for tissue regeneration and volume retention. Acta Biomater. 2022;142:73–84.
57. Tezel A, Fredrickson GH. The science of hyaluronic acid dermal fillers. J Cosmet Laser Ther. 2008;10(1):35–42.
58. Faivre J, Pigweh AI, Iehl J, et al. Crosslinking hyaluronic acid soft-tissue fillers: current status and perspectives from an industrial point of view. Expert Rev Med Dev. 2021;18(12):1175–87.
59. Murray G, Convery C, Walker L, et al. Guideline for the management of hyaluronic acid filler-induced vascular occlusion. J Clin Aesthet Dermatol. 2021;14(5):E61.
60. Soares DJ. Bridging a century-old problem: the pathophysiology and molecular mechanisms of HA filler-induced vascular occlusion (FIVO)—implications for therapeutic interventions. Molecules. 2022;27(17):5398.
61. Schoof H, Apel J, Heschel I, et al. Control of pore structure and size in freeze-dried collagen sponges. J Biomed Mater Res. 2001;58(4):352–7.
62. Park H, Guo X, Temenoff JS, Tabata Y, et al. Effect of swelling ratio of injectable hydrogel composites on chondrogenic differentiation of encapsulated rabbit marrow mesenchymal stem cells in vitro. Biomacromolecules. 2009;10(3):541–6.

63. Pierre S, Liew S, Bernardin A. Basics of dermal filler rheology. Dermatol Surg. 2015;41:S120–6.
64. Jarquín-Yáñez K, Herrera-Enríquez MÁ, Benítez-Barrera DI, et al. Subcutaneous application of a Gelatin/Hyaluronic acid hydrogel induces the production of skin extracellular matrix. Polymers. 2024;16(5):573.
65. Chouhan D, Dey N, Bhardwaj N, et al. Emerging and innovative approaches for wound healing and skin regeneration: current status and advances. Biomaterials. 2019;216:119267.
66. Qu J, Zhao X, Liang Y, et al. Degradable conductive injectable hydrogels as novel antibacterial, anti-oxidant wound dressings for wound healing. Chem Eng J. 2019;362:548–60.
67. Qin K, Wang F, Simpson RML, et al. Hyaluronan promotes the regeneration of vascular smooth muscle with potent contractile function in rapidly biodegradable vascular grafts. Biomaterials. 2020;257:120226.
68. Harper RA, Grove G. Human skin fibroblasts derived from papillary and reticular dermis: differences in growth potential in vitro. Science. 1979;204(4392):526–7.
69. He K, Zhang X, Ren S, et al. Deep residual learning for image recognition//proceedings of the IEEE conference on computer vision and pattern recognition. 2016. p. 770–8.
70. Kandyel RM, Elwan MM, Abumandour MMA, et al. Comparative ultrastructural-functional characterizations of the skin in three reptile species; Chalcides ocellatus, Uromastyx aegyptia aegyptia, and Psammophis schokari aegyptia (FORSKAL, 1775): adaptive strategies to their habitat. Microsc Res Tech. 2021;84(9):2104–18.
71. Kashimoto R, Furukawa S, Yamamoto S, et al. Lattice-patterned collagen fibers and their dynamics in axolotl skin regeneration. Iscience. 2022;25(7):104524.
72. Hahn, Hyung M, Woo BL, JLee I. The effects of subcutaneously injected novel biphasic cross-linked hyaluronic acid filler: in vivo study. Aesthetic Plast Surg. 2021;45:322–31.